Supporting Information

High Energy Density Micro-Supercapacitor based on Three-Dimensional Bicontinuous Porous Carbon with Interconnected Hierarchical Pore

Xinyu Ma, [a] Xufeng Hong, [a] Liang He, [*a,b] Lin Xu, [a] Yanjia Zhang, [a] Zhe Zhu, [a] Xuelei Pan, [a] Jiexin Zhu, [a] Liqiang Mai[*a]

[a]State Key Laboratory of Advanced Technology for Materials Synthesis and Processing, Wuhan University of Technology, Wuhan 430070, P. R. China

[b]Department of Materials Science and NanoEngineering, Rice University, Houston, TX 77005, United States

*Corresponding Authors.

E-mail: hel@whut.edu.cn (Prof. Liang He); mlq518@whut.edu.cn (Prof. Liqiang Mai).

Note 1:

Preparation of ZnO nanowires and ZnO nanoparticles. ZnO nanowires were synthesized by hydrothermal method as reported previously.[1] A clarified aqueous solution was obtained by mixing 0.4 g ZnCl • $6H_2O$ and 20 g Na_2CO_3 in 45 mL deionized (DI) water, followed by stirring for 15 min. Then the solution was transferred to a Teflon autoclave and reserved at 120 °C for 14 h. The ZnO nanowires were obtained after cleaning the product with DI water for three times and drying at 80 °C for 12 h. ZnO nanoparticles were prepared by annealing precursor synthesized by coprecipitation method.[2] In the synthesis of ZnO nanoparticles, $Zn(NO_3)_2$ aqueous solution (1.5 mol L^{-1}) was dropped slowly to $(NH_4)CO_3$ aqueous solution (2.25 mol L^{-1}) with continuously and tempestuously stirring to obtain the precursor. After annealing the precursor at 500 °C in the air for 2 h, ZnO nanoparticles were obtained.

Microfabrication of carbon-based MSC activated by ZnO. Carbon-based MSC was fabricated by optimized C-MEMS process. The ZnO/photoresist composite was obtained by stirring and ultra-sonication of ZnO in PR1-9000A photoresist for 6 h. Then, ZnO/photoresist thin film on Si/SiO_2 substrate was prepared by two-step spin coating (1000 rmp for 10 s, then 4000 rmp for 40s) of ZnO/photoresist composite. Photolithography with a dose of 950 mJ cm^{-2} was conducted to expose the sample after pre-baking at 100 °C for 15 min, and the fingers micropattern was obtained by development in RD6 developer. The following carbonization and activation processes were performed in cube stove under N_2 atmosphere (N_2 flow rate: 50 cc min^{-1}). The temperature of cube stove increased to 300 °C at a rate of 2 °C min^{-1} and remained at 300 °C for 30 min for solidification. Then, the carbonization of photoresist and activation of that by ZnO were performed at 900 °C for 1 h. What's note is that with the increase of ZnO in weight percent, the viscosity of composite increases, which means that several drops of diluent should be added into the composite.

Materials characterization. XRD was employed to characterize the crystallographic information of samples using a Bruker D8 Advance X-ray diffractometer with a nonmonochromated Cu Kα X-ray source. SEM images and energy dispersive spectroscopy (EDS) results were collected with a JEOL-7100F SEM/EDS microscope at an acceleration voltage of 20 kV. TG/differential scanning calorimeter (DSC) was performed using a Netzsch STA 449C simultaneous thermal analyzer at a heating rate of 10 °C min^{-1} in N_2 atmosphere. Raman spectra were recorded through a Renishaw inVia Raman microscope, and a 532 nm He-Ne laser was focused on the samples.

Measurement of electrochemical performance. The electrochemical performance of MSCs was measured by electrochemical workstation (Autolab PGSTAT 302N) using two-electrode system. 0.08 M KI electrolyte and 20 M LiTFSi were prepared according to the procedure reported in the reference.[3-4] The areal capacitance (in F cm^{-2}) is calculated using the following equation.

$$Cs = \frac{\int I \mathrm{d}V}{v \times (\Delta V) \times S}$$

Where I is the current (in A), v is the scan rates (in V s^{-1}), ΔV is the operation potential window (in V), and S is the total areal (in cm^{-2}) of the MSC.

The energy density (E, in Wh cm^{-2}) and power density (P, in W cm^{-2}) of the MSC are calculated by following equations.

$$E = \frac{Cs \times (\Delta V)^2}{7200}$$

$$P_{av} = \frac{E}{\Delta t} \times 3600$$

Where C_s (in F cm^{-2}) is the volume capacitance obtained from equation (1) and Δt is the discharge time of the MSC (in seconds).

Note 2:

The areal atomic ratio:

With powder or other porous materials, the capacitance ideally scales with the available surface while the weight scales with the volume. The equivalent series resistance will be determined by pores' lengths and diameters, as well as their distribution in relation to the accessibility of pores and voids to the supporting electrolyte having a given conductivity. Here, if the influence of pore structure is not considered, in the per volume, the more surface area means the more capacitance during cycling, which also needs more electron transforming. However, the decrease of value of carbon atoms will limit the electrical conductivity. Hence, the areal atomic ratio refers to the degree of coordination in ion and electron transformation.

The ohmic accumulation:

In porous electrode materials for electrochemical capacitors, there is usually a tradeoff between porosity and pore size. Percent porosity normally diminishes as pore size decreases, but the relation between these quantities depends on the pore-size distribution and the type of carbonaceous materials from which the porous carbon was derived. For porous capacitor electrodes, the requirements are: (1) sufficient volume for accommodation of electrolyte; (2) provision of electrolyte pathways to access surface area and thus to maximize conductivity of electrolyte-flooded matrix, and (3) optimization for maximizing specific area for development of the highest realizable double-layer capacitance per square centimeter or per gram. After infiltrated by electrolyte, the pore delivers the ion resistance inside. As the general knowledge, the diameter of electrolyte has positive correlation with ion conductivity of this pore structure.
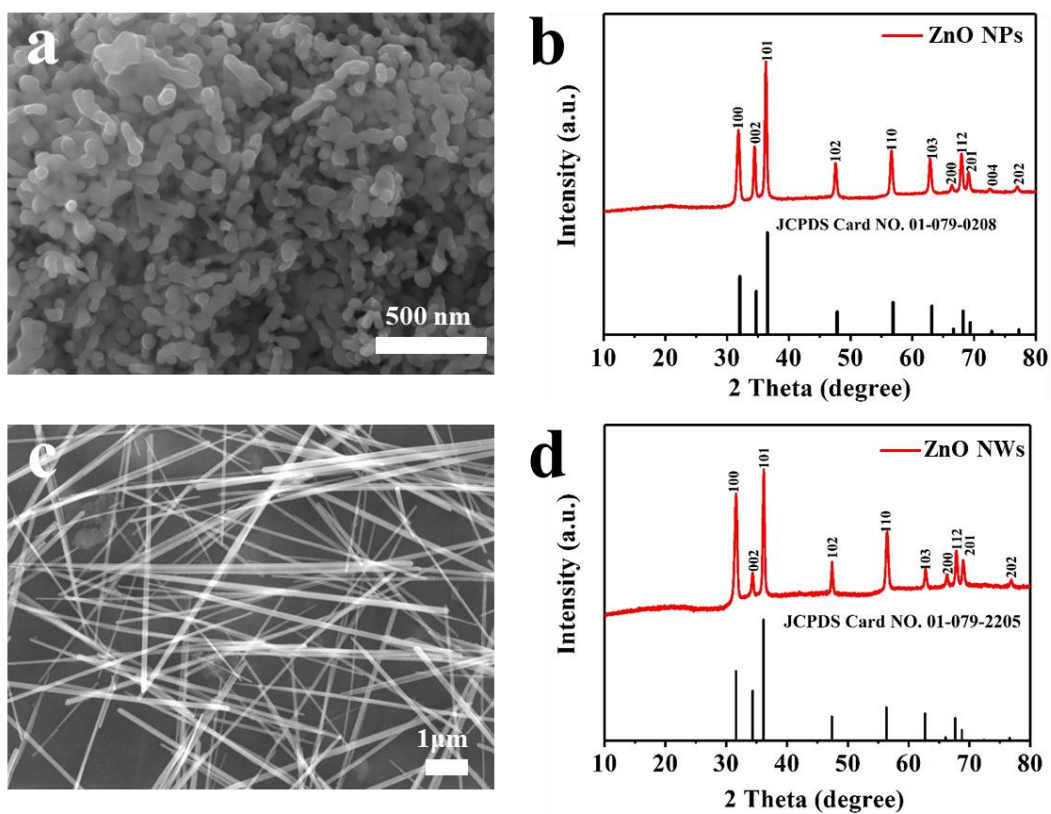
Figure S1. SEM images of a) ZnO NPs and c) ZnO NWs. XRD patterns of b) ZnO NPs and d) ZnO NWs, respectively.
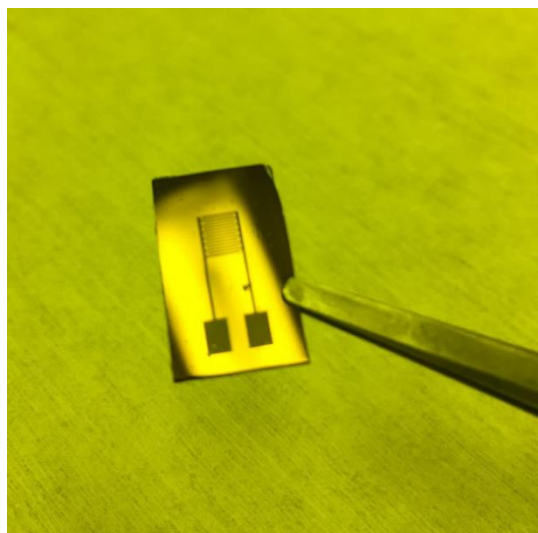
Figure S2. Optical images of pyrolyzed carbon based MSC activated by 15 wt. % ZnO NWs. The area of the interdigital microelectrodes is 0.0927 cm^2.
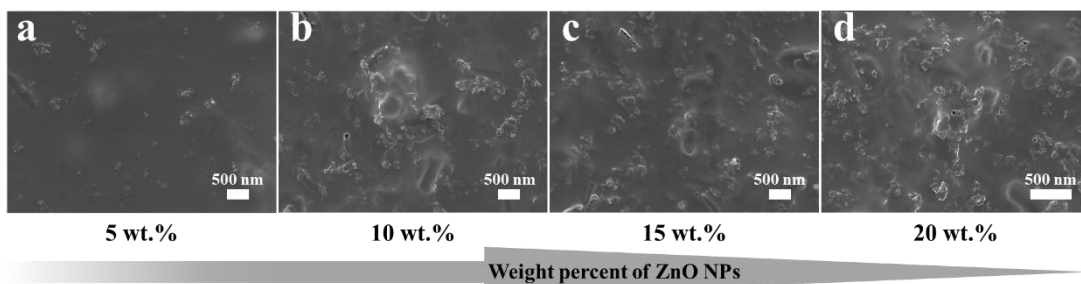
Figure S3. SEM images of carbon-based microelectrodes activated by a) 5 wt. %, b) 10 wt. %, c) 15 wt. %, and d) 20 wt. % ZnO NPs, respectively.
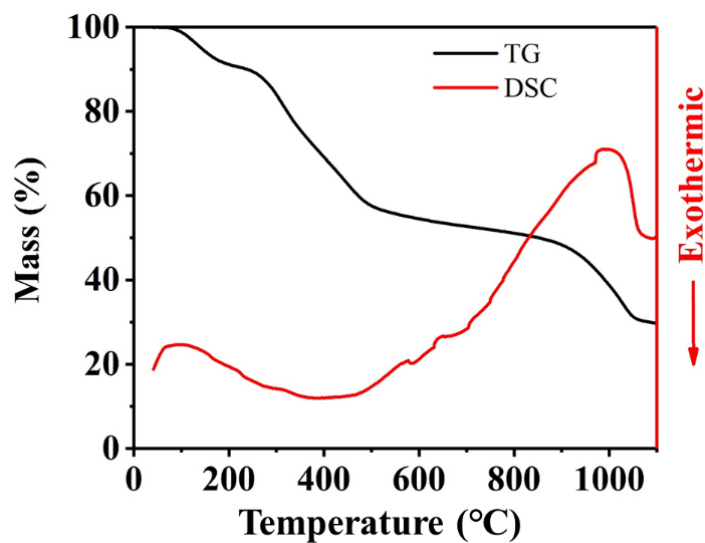
Figure S4. TG-DSC curves of 15 wt. % ZnO NWs/photoresist.
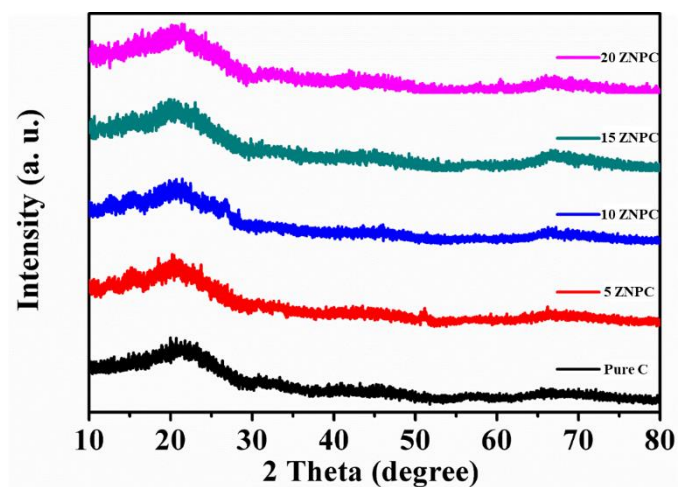
Figure S5. XRD patterns of carbon-based microelectrodes activated by 0 wt. %, 5 wt. %, 10 wt. %, 15 wt. % and 20 wt. % ZnO NPs, respectively.
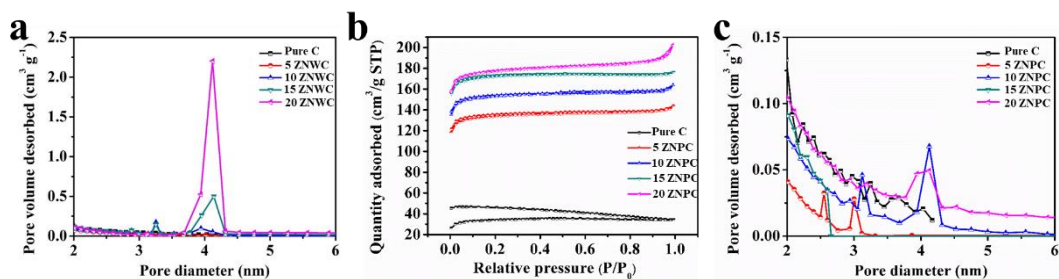
Figure S6. a) Pore structure of carbon-based microelectrodes activated by 0 wt. %, 5 wt. %, 10 wt. %, 15 wt. % and 20 wt. % ZnO NWs, respectively. b) BET adsorption-desorption curves. c) Pore structure of carbon-based microelectrodes activated by 0 wt. %, 5 wt. %, 10 wt .%, 15 wt. % and 20 wt. % ZnO NPs, respectively.
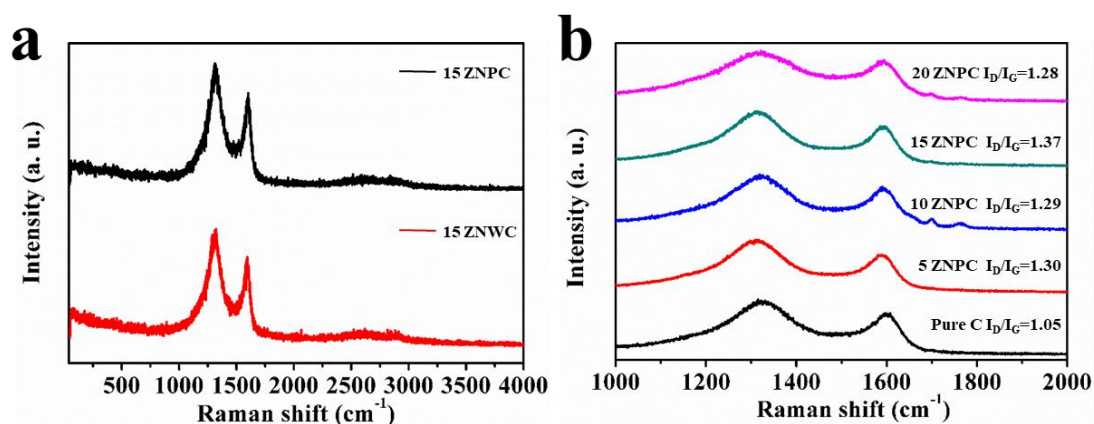
Figure S7. Raman spectra of carbon-based microelectrodes activated by a) 15 wt. % ZnO NPs and 15 wt. % ZnO NWs, and b) 0 wt. %, 5 wt. %, 10 wt. %, 15 wt. % and 20 wt. % ZnO NWs, respectively.
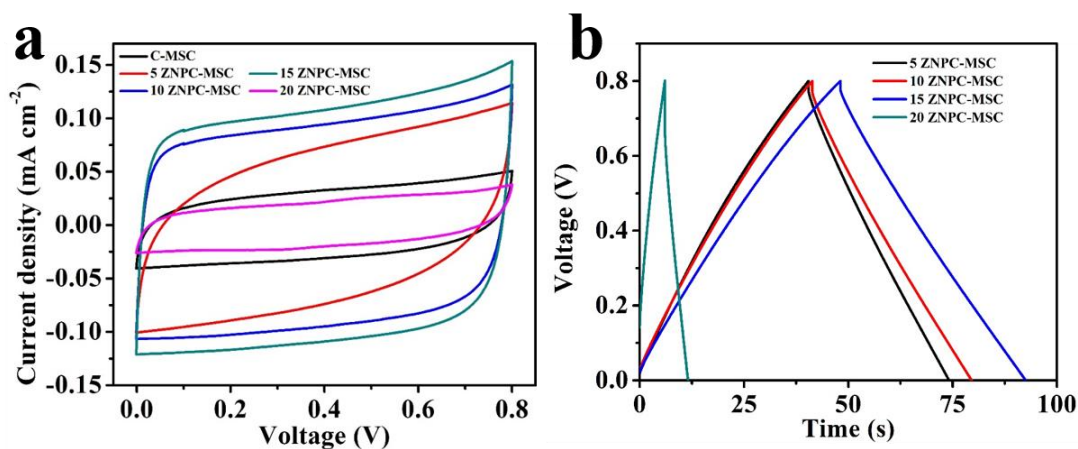
Figure S8. a) CV curves at the scan rate of 20 mV s^{-1} and b) GCDC curves of C-MSC and 5-20 ZNPC-MSCs at the current density of 0.1 mA cm^{-2}.
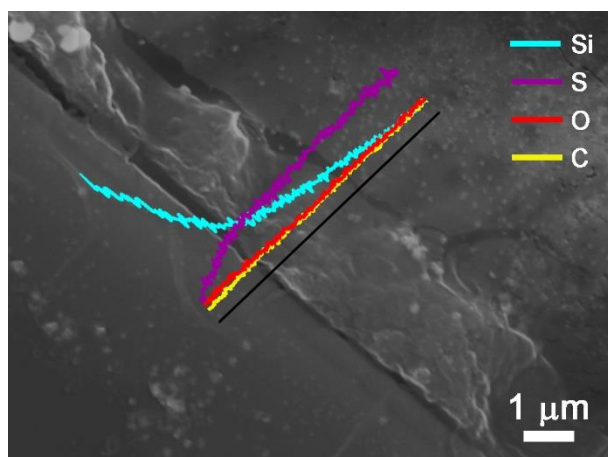
Figure S9. EDS line scan spectra of carbon based microelectrode activated by 15 wt. % ZnO NWs with H$_2$SO$_4$-PVA (In the supporting information).
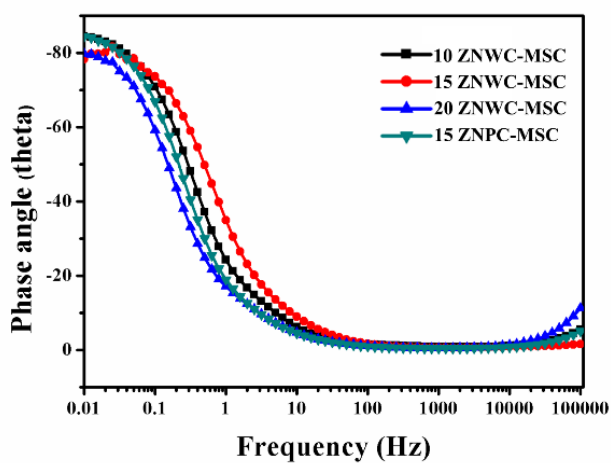
Figure S10. Bode plots of impedance of 10 ZNWC-MSC, 15 ZNWC-MSC, 20 ZNWC-MSC and 15 ZNPC-MSC.
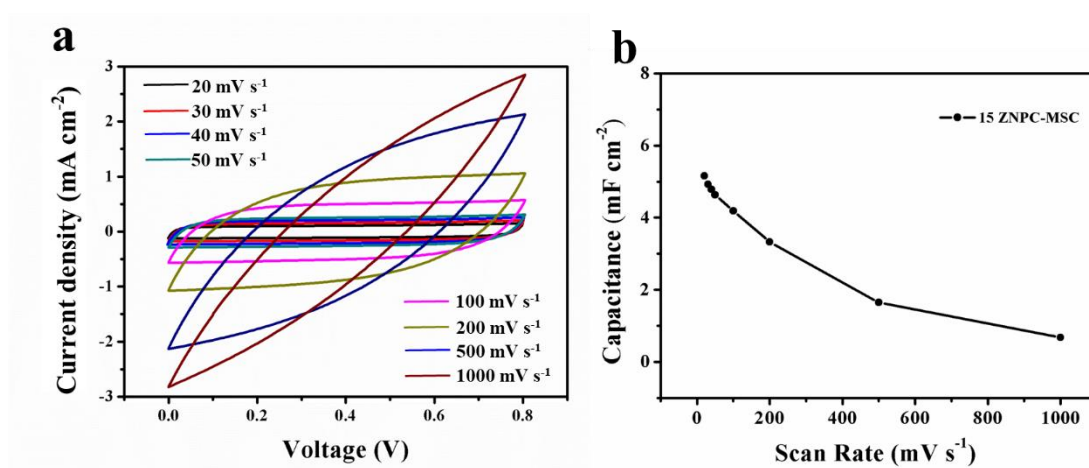
Figure S11. a) CV curves and b) rate performance of 15 ZNPC-MSCs.
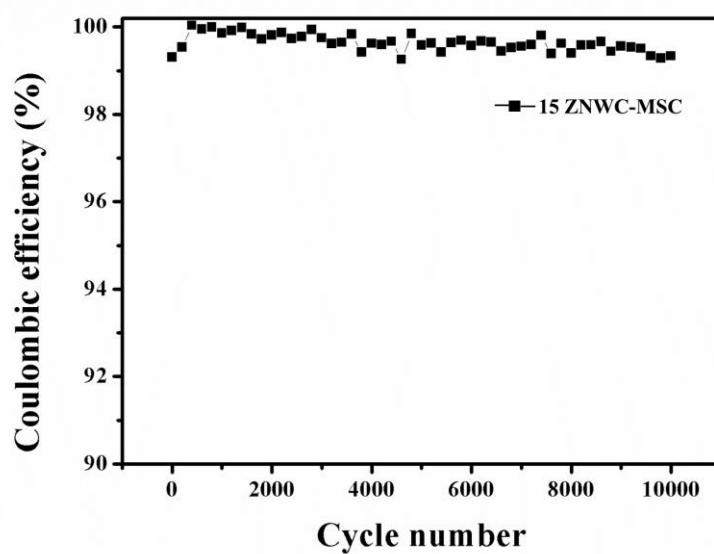
Figure S12. Coulombic efficiency of 15 ZNWC-MSC in cycling process.
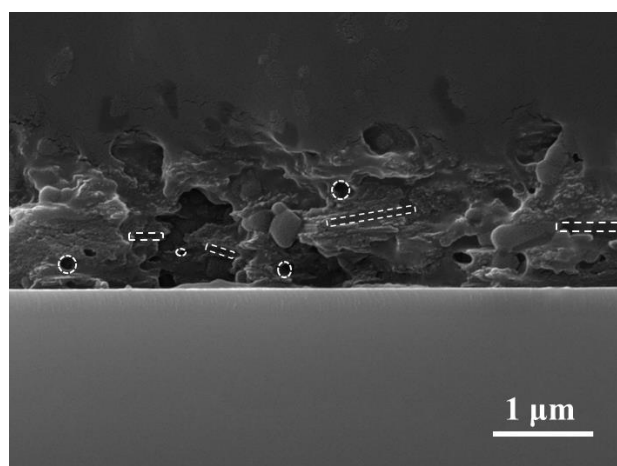
Figure S13. SEM image of 15 ZNWC-MSC after cycling process.
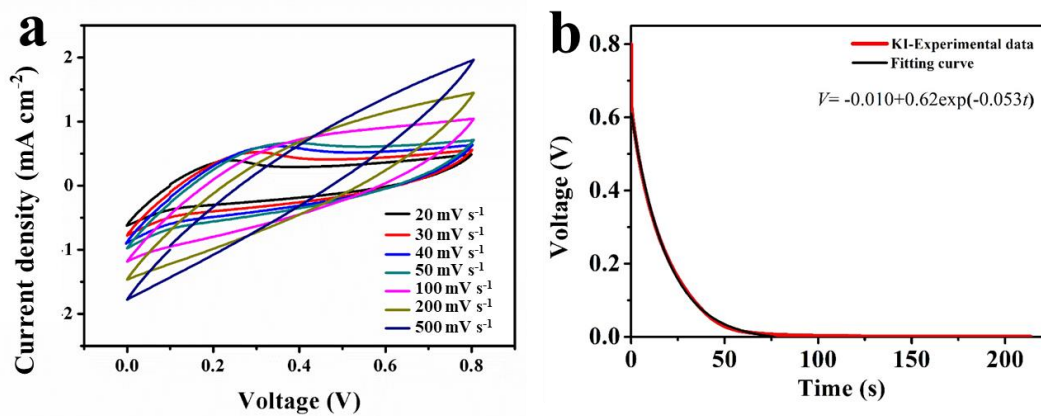
Figure S14. a) CV curves and b) self-discharge curve and fitting curve of KI-MSC.
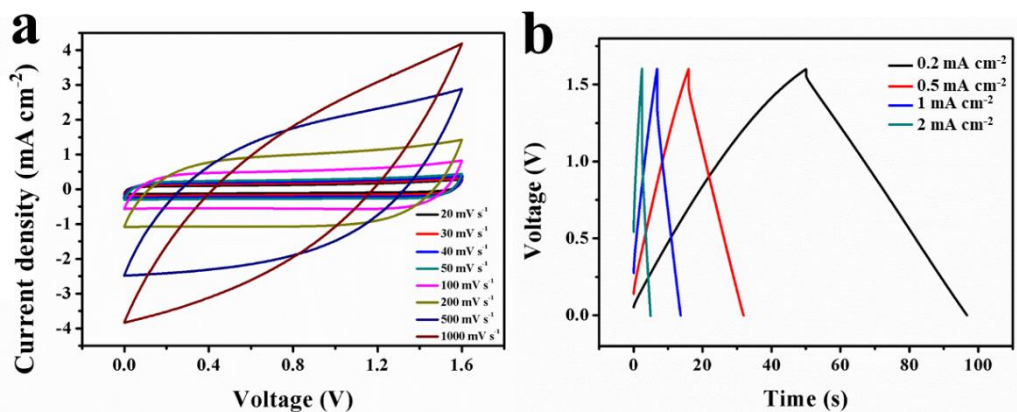
Figure S15. a) CV curves and b) GCD curves of LiCl-MSC.
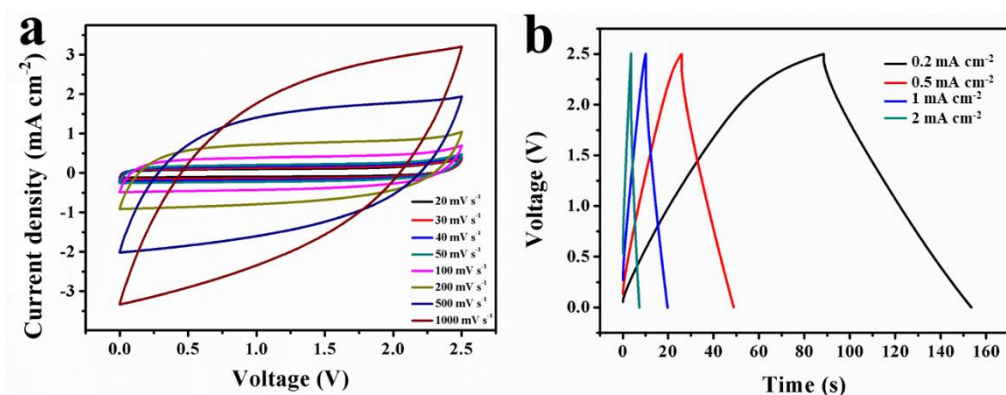
Figure S16. a) CV curves and b) GCD curves of LiTFSi-MSC.
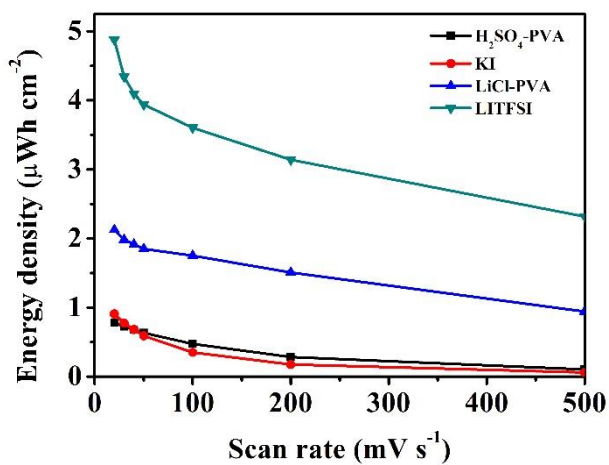
Figure S17. The rate performance of 15 ZNWC-MSCs with different electrolytes (*vs.* energy density).

Table S1. SSA values of carbon-based microelectrodes.

The content of ZnO (wt.%)	BET surface area of pyrolyzed carbon activated by ZnO NWs ($m^2\ g^{-1}$)	BET surface area of pyrolyzed carbon activated by ZnO NPs ($m^2\ g^{-1}$)
0	109.1223	109.1223
5	403.6788	284.7044
10	510.4249	424.8861
15	649.3826	545.7464
20	790.8275	563.0895

Table S2. The IR drop of ZNWC-MSCs and ZNPC-MSCs.

The content of ZnO (wt.%)	IR drop of ZNWC-MSCs (mV)	IR drop of ZNPC-MSCs (mV)
5	10.98	26.55
10	11.29	27.47
15	25.63	22.58
20	32.35	140.99

Table S3. The specific areal capacitances of ZNWC-MSCs and ZNPC-MSCs.

The content of ZnO (wt.%)	Specific areal capacitance of ZNWC-MSCs ($mF\ cm^{-2}$)	Specific areal capacitance of ZNPC-MSCs ($mF\ cm^{-2}$)
0	1.42	1.42
5	5.86	3.97
10	8.44	4.46
15	8.83	5.51
20	4.69	0.93

Table S4. Comparison of fabrication method, active material, electrochemical performance of various MSCs

Fabrication method	Material	Capacitance (Areal capactitance: $mF\ cm^{-2}$ / Volumn capacitance: $F\ cm^{-3}$)	Energy density (Areal energy density: $\mu Wh\ cm^{-2}$ / Volumn energy density: $mWh\ cm^{-3}$)
Full inkjet-printing[5]	Electrochemically exfoliated graphene	0.7 / ~10	0.04 / 1
Spread and laser writing[6]	Graphene/ Au composite	3.84 / 20	0.53 / No mentioned
Lignin laser lithography and	3D graphene/Au composite	25.1 / 6.27	2.6 / ~1

soak[7]			
Freeze-drying and laser writing[8]	Cellular graphene films	2.47 / 1.27	0.34 / 0.17
Hydrothermal, repeated spin coating and photolithography [9]	MoS$_2$ nanosheets @rGO-CNTs	13.7 / 40	1.9 / 5.6
Four beam interference lithography[10]	Pyrolysis carbon	5.9 / 11	1.57 / 1.43
Vacuum filtration and laser cutting [11]	Few-layered MXene	71.16 / 151.1	3.52 / 7.48
Stamping[12]	MXene inks	61 / no mentioned	0.63 / no mentioned
Screen printing and electrodeposition [13]	MnO$_2$//PPy	25.8 / no mentioned	8.05 / no mentioned
Inkjet print and electrodeposition [14]	MnO$_2$ on 3D Ni collector	52.9 / 152	3.51 / 13.0
Hydrothermal and photolithography (this work)	Three-dimensional bicontinuous porous carbon	**5.62/ 20.06**	**4.9 / 11.3**

Reference:

1. Hu H.; Huang X.; Deng C.; Chen X.; Qian Y., Hydrothermal Synthesis of ZnO Nanowires and Nanobelts on a Large Scale, *Mater. Chem. Phys.* 2017, 106(1), 58-62.
2. Davood R.; Synthesis and Microstructural Properties of ZnO Nanoparticles Prepared by Precipitation Method, *Renew. Energy* 2013, 50, 932-937.
3. Senthilkumar S.; Kalai S.; Lee Y.; Melo J., Electric Double Layer Capacitor and its Improved Specific Capacitance Using Redox Additive Electrolyte, *J. Mater. Chem. A* 2013, 1, 1086-1095.
4. Suo L.; Borodin O.; Gao T.; Olguin M.; Ho J.; Fan X.; Luo C.; Wang C.; Xu K., "Water-in-Salt" Electrolyte Enables High-Voltage Aqueous Lithium-Ion Chemistries. *Science* 2015, 350(6263), 938-943.
5. Li J.; Delekta S.; Zhang P.; Yang S.; Lohe M.; Zhuang X.; Feng X.; Östling M., Scalable Fabrication

and Integration of Graphene Microsupercapacitors through Full Inkjet Printing, *ACS Nano* 2017, 11(8) , 8249-8256.

6. Li R.; Peng R.; Kihm K.; Bai S.; Bridges D.; Tumuluri U.; Wu Z.; Zhang T.; Compagnini G.; Feng Z.; Hu A., High-Rate In-Plane Micro-Supercapacitors Scribed onto Photo Paper Ssing In Situ Femtolaser-Reduced Graphene Oxide/Au Nanoparticle Microelectrodes. *Energy Environ. Sci.* 2016, 9(4), 1458-1467.

7. Zhang W.; Lei Y.; Ming F.; Jiang Q.; Costa P.; Alshareef H., Lignin Laser Lithography: A Direct-Write Method for Fabricating 3D Graphene Electrodes for Microsupercapacitors. *Adv. Energy Mater.* 2018, 8(27), 1801840.

8. Shao Y.; Li J.; Li Y.; Wang H.; Zhang Q.; Kaner R., Flexible Quasi-Solid-State Planar Micro-Supercapacitor based on Cellular Graphene Films. *Mater. Horiz.* 2017, 4(6), 1145-1150.

9. Yang, W.; He, L.; Tian, X.; Yan, M.; Yuan, H.; Liao, X.; Meng, J.; Hao, Z.; Mai, L., Carbon-MEMS-Based Alternating Stacked MoS_2@rGO-CNT Micro-Supercapacitor with High Capacitance and Energy Density. *Small* 2017, 13(26), 1700639.

10. Kim C.; Moon J., Hierarchical Pore-Patterned Carbon Electrodes for High Volumetric Energy Density Microsupercapacitors. *ACS Appl. Mater. Inter.* 2018, 10(23), 19682-19688.

11. Hu H.; Bai Z.; Niu B.; Wu M.; Hua T., Binder-Free Bonding of Modularized MXene Thin Films into Thick Film Electrodes for On-Chip Micro-Supercapacitors with Enhanced Areal Performance metrics. *J. Mater. Chem. A* 2018, 6(30), 14876-14884.

12. Zhang C.; Kremer M.; Seral-Ascaso A.; Park S.; McEvoy N.; Anasori B.; Park S.; McEvoy N.; Anasori B.; Gogotsi Y.; Nicolosi, V., Stamping of Flexible, Coplanar Micro-Supercapacitors Ssing MXene Inks. *Adv. Fun. Mater.* 2018, 28(9), 1705506.

13. Guo, R.; Chen, J.; Yang, B.; Liu, L.; Su, L.; Shen, B.; Yan, X., In-Plane Micro-Supercapacitors for an Integrated Device on One Piece of Paper. *Adv. Fun. Mater.* 2017, 27, 1702394.

14. Lin Y.; Gao Y.; Fan Z., Printable Fabrication of Nanocoral-structured electrodes for high-Performance Flexible and Planar Supercapacitor with Artistic Design. *Adv. Mater.* 2017, 29(43), 1701736.